# A high-performance TPGDA/PETEA composite gel polymer electrolyte for lithium metal batteries

Zhifu Chen,[a] Quan Pei,[a] Zhitao An,[a] Yiting Tong,[a] Qingfeng Zhang,[*b] Shuhong Xie[*a]

a. Key Laboratory of Low Dimensional Materials and Application Technology of Ministry of Education, School of Materials Science and Engineering, Xiangtan University, Xiangtan 411105, P. R. China;

b. Hunan Provincial Key Laboratory of Thin Film Materials and Devices, School of Materials Science and Engineering, Xiangtan University, Xiangtan 411105, P. R. China.

E-mail: zhangqf@xtu.edu.cn, shxie@xtu.edu.cn

## 1. Experimental section

### *1.1 Preparation of materials*

The precursor solution consisted of 2 wt% polymer monomers and 0.1 wt% 2,2'-Azobis(2-methylpropionitrile) (AIBN, Aladdin, 99%) as initiator in the liquid electrolyte, which is 1.0 M $LiPF_6$ in EC:DMC:EMC = 1:1:1 vol%. Polymer monomers included Tripropylene Glycol Diacrylate (TPGDA, Aladdin, 90%) and Pentaerythritol Tetraacrylate (PETEA, Aladdin, 80%) in a 1:1 ratio. Dissolved the polymer monomers and initiator in the electrolyte and stirred for 30 mins. LLZTO powders was purchased from HF-Kejing. Dimethylacetamide (DMAC, 99%) was purchased from Sinopharm Chemical Reagent Co. Ltd. 1,2,4,5-Benzenetetracarboxylic anhydride (PMDA, 99%) and 4,4-oxybisbenzenamine (ODA, 98%) were purchased from Aladdin.

### *1.2 Preparation of PI/LLZTO/GPE, PI/GPE and PP/GPE*

The PI/LLZTO/GPE was obtained according to the following steps: Firstly, ODA was added to DMAC and stirred continuously until dissolved completely. Then, LLZTO was added into the solution, followed by the addition of PMDA. After stirring for 24 h, a polyamide acid (PAA) solution with 20 wt% was obtained. The ratio of ODA to PMDA was 1:1, and the content of LLZTO was 1 wt%. Secondly, the PAA solution was used as the precursor solution for electrospinning, the high voltage was 20 kV, the distance between the needle and the collecting plate was about 16 cm, and the propulsion speed was 1 mL $h^{-1}$. Then, the nanofiber membranes obtained by electrospinning were put into muffle furnace and imidized at 100 ℃, 200 ℃, 300 ℃ for 2 h, respectively. Finally, the 60 μL precursor solution was dripped onto the dry nanofiber membranes (d = 16 mm) placed on the glass plate, then covered another glass plate so that the precursor solution was spread on the surface of the membranes evenly; the precursor solution was completely polymerized by heated to 60 ℃ for 2 h, and then the PI/LLZTO/GPE was obtained. For comparison, composite gel polymer electrolytes supported on pure PI nanofiber membranes (PI/GPE) and commercial polypropylene (PP/GPE) were prepared by the same method.

### *1.3 Preparation of LFP cathode and Li|electrolyte|LFP cell*

Firstly, a certain amount of poly(vinylidene fluoride) (PVDF) was added into 1-methyl-2-pyrrolidi-none (NMP, Aladdin), stirred continuously until the PVDF was dissolved completely, then added the mixed powder of LFP and Ketjen Black (KB, ECP-300J) (LFP:PVDF:KB = 8:1:1), and stirred for 6 h to get a homogeneous cathode slurry. Subsequently, the cathode slurry was poured on Al foil and coated evenly with the scraper, then heated to 80 ℃ for 12 h in vacuum to remove the solvent completely. The mass loading of the LFP cathode was about 1.3 mg $cm^{-2}$. Afterwards, the precursor solution was dripped onto the nanofiber membranes (d = 16 mm) that was placed on a piece of Li metal in a CR2032 coin-type cell, and then the LFP cathode was placed on top of it. After completely packaging, the cell passed by the same polymerization process by heated to 60 ℃ for 2 h. The Li|PI/GPE|LFP and Li|PP/GPE|LFP cell was assembled by the same process. In this paper, all types of cells for testing were assembled using this similar method of in-suit polymerization on different electrodes.

*1.4 Materials characterization*

The bonding structure of electrolyte before and after polymerization was studied by Fourier transform infrared spectrometer (FTIR, Nicolet IS 5). A field-emission scanning electron microscopy (FESEM, FEI Apreo S LoVac) was used for morphology testing. The phase structure of the nanofiber membranes and electrolytes were analyzed via X-ray diffraction (XRD) with Rigaku U 1 tima IV (Cu Kα) in a 2θ range of 10-80°.

*1.5 Electrochemical characterization*

The electrochemical impedance spectroscopy (EIS) of different types cells were obtained by CHI1600D electrochemical workstation, the recorded frequencies were $10^{-1}$~$10^{6}$ Hz and the AC amplitude was 10 mV. The geometric area of the LFP cathode and GPE was about 1.13 $cm^{-2}$ and 2.01 $cm^{-2}$, respectively. The ionic conductivity ($\sigma$) of electrolytes were obtain by assembled blocking cells with two stainless steel electrodes (SS). According to the bulk resistance ($R$) of the electrolyte obtained from Nyquist curve, the ionic conductivity ($\sigma$) can be calculated by the following equation:[1]

$$\sigma = \frac{L}{RA} \tag{1}$$

where $L$ and $A$ represent the thickness of the electrolyte and the area of SS electrode, respectively. The $Li^+$ transference number ($t_{Li+}$) of electrolytes was measured by using a symmetrical Li|electrolyte|Li cells combined with EIS analysis and DC polarization. Use the following Bruce-Vincent equation to calculate $t_{Li+}$:[2]

$$t_{Li+} = \frac{I_s(\Delta V - I_o R_o)}{I_o(\Delta V - I_s R_s)} \tag{2}$$

where the polarization potential $\Delta V$ is 10 mV, $R_o$ and $R_s$ represent the interfacial resistance before and after polarization, $I_o$ and $I_s$ represent the initial and stable current, respectively. By using linear sweep voltammetry (LSV) for Li|electrolyte|SS cells from open-circuit voltage to 6 V range under 0.1 mV $s^{-1}$ scanning rate the electrochemical stability window was evaluated. Cyclic voltammograms (CV) of Li|electrolyte|LFP cell were executed also at 0.1 mV $s^{-1}$ scanning rate. The galvanostatic charging-discharging of cells was performed in NEWARE CT-4008T battery testing system. The symmetrical Li cells is plated and stripped under the current density of 0.5 mA

$cm^{-2}$ for 1 h per cycle, and the voltage range of Li|electrolyte|LFP cells for testing is from 2.5 to 4.2 V.

## 2. Results and discussion

Fig. S1. shows the fabrication procedures of the PI/LLZTO/GPE membranes. Although the ionic conductivity of PI skeleton film is small, the addition of LLZTO and precursor electrolyte can fill its numerous pores fully, which makes it have high ionic conductivity. After polymerization, a composite gel polymer electrolyte with LLZTO dispersed uniformly on PI based was obtained, as shown in the schematic of Fig. S1.

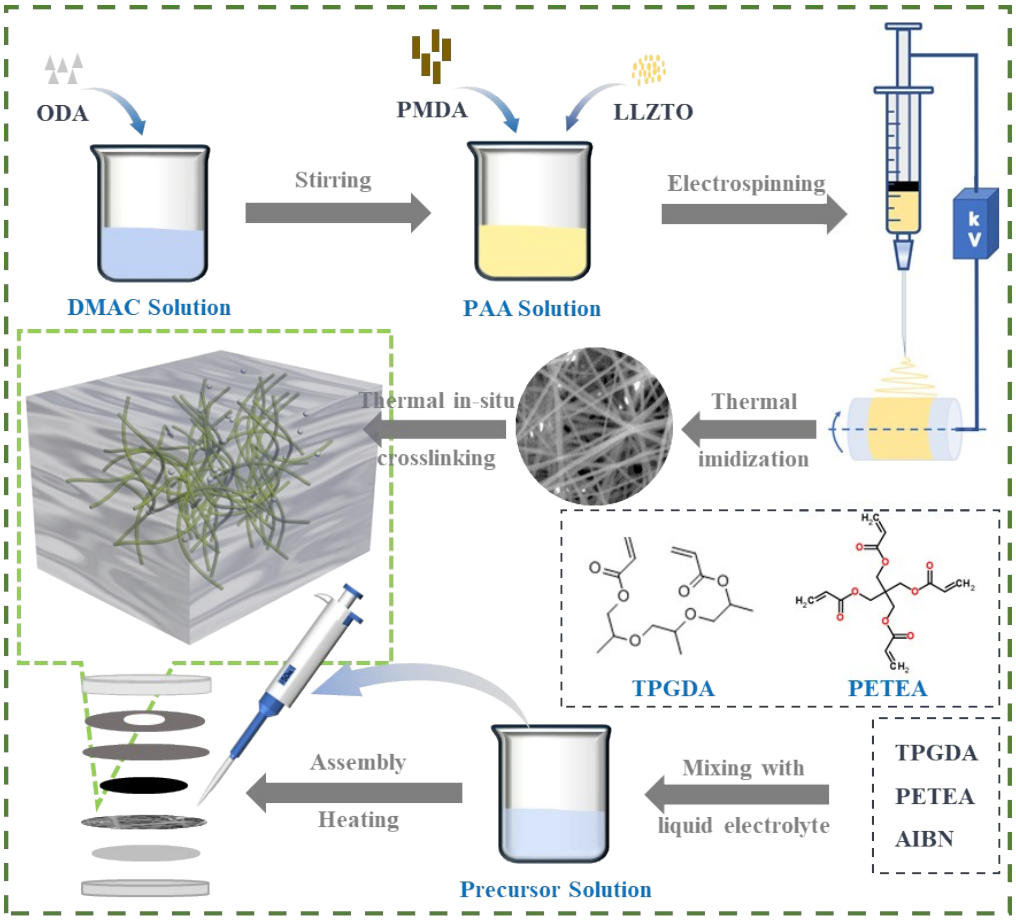


**Fig. S1.** The preparation schematic of the PI/LLZTO/GPE.

Fig.S2a shows the excellent flexibility of the PI/LLZTO/GPE membranes, which can recover to the initial appearance after bending and folding, and the surface remains intact after unfolding. This is mainly attributed to the PI/LLZTO nanofiber membrane, which provides good flexibility and a self-supporting skeleton for the precursor electrolyte. It is benificial to overcome the inherent brittleness after polymerization of acrylate monomers, thereby obtain a gel polymer electrolyte with excellent flexibility. The optical photos in Fig. S2b shows the transformation of precursor electrolyte from liquid to solid during the process of solidification. Equal amounts of TPGDA and PETEA monomers are mixed with the liquid electrolyte at a ratio of 2%. As a thermal initiator, AIBN decomposes and generates free radicals at 60 °C. Under the effect of free radicals, the unsaturated C=C bonds in the monomers undergo the opening and polymerization steps. During this process, the clarified precursor electrolyte turns into a milky white translucent solid slowly, and the electrolyte also blocks the liquid plasticizer (EC/DMC/EMC-$LiPF_6$),

providing a pathway for the rapid transmission of $Li^+$.

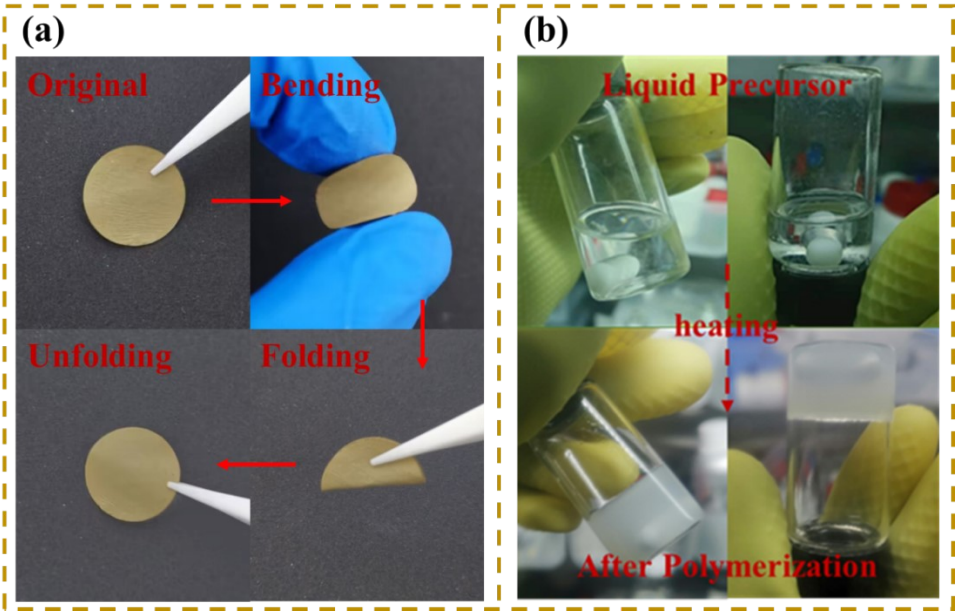


**Fig. S2.** (a) Photographs of the PI/LLZTO/GPE under bending and folding states; (b) In-situ polymerization process of liquid precursor under heating at 60 ℃ for 2 h.

The comparative XRD patterns in Fig. S3a indicate that the peaks of initial LLZTO and LLZTO in PI/LLZTO are consistent with that of JCPDS card (PDF#01-090-2954) corresponding LLZTO ceramic, the cubic phase structure of LLZTO is stable under thermal imidization and polymerization processes. Fig. S3b shows the FTIR results of PI/LLZTO, PI/LLZTO/GPE membrane and monomers. PI/LLZTO has a series of characteristic peaks, including the symmetric and asymmetric tensile vibrations of carbonyl group in the imine ring at 1716 $cm^{-1}$ and 1775 $cm^{-1}$, respectively. The tensile vibration of C-N bond at 1371 $cm^{-1}$ and the peak at 819 $cm^{-1}$ are the variable angle vibration of C=O bond and the deformation vibration of imine ring.[2] These peaks prove that the presence of LLZTO powders does not affect the formation of PI membrane. There is no C=C peak in the PI/LLZTO/GPE characteristic peak, which further indicates that the polymerization is formed by the C=C fracture.[3] The characteristic peak of PI/LLZTO/GPE is almost coincides with that of PI/LLZTO except for a new peak at 1378 $cm^{-1}$, which related to the C-H bending vibration generated by saturated hydrocarbon groups.

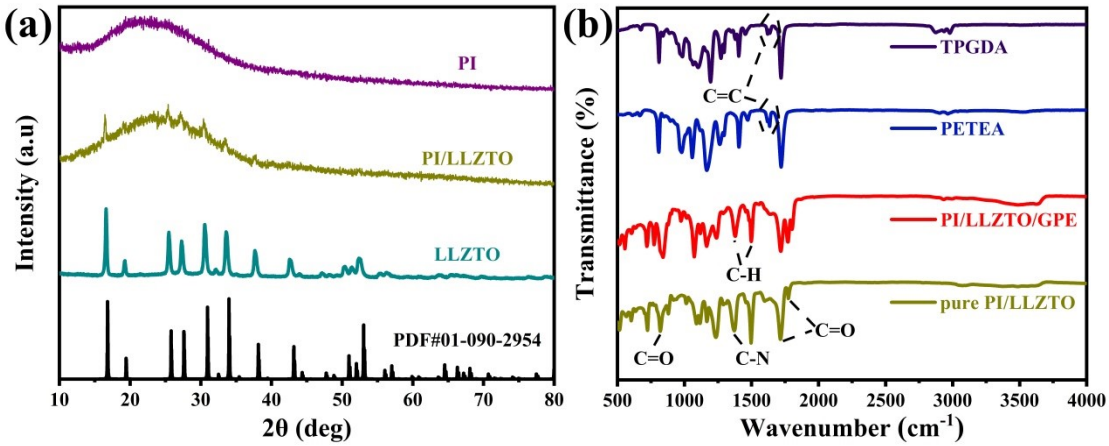


**Fig. S3.** (a) FTIR spectra of TPGDA, PETEA, PI/LLZTO/GPE and PI/LLZTO membrane; (b) XRD patterns of PI, PI/LLZTO and LLZTO.

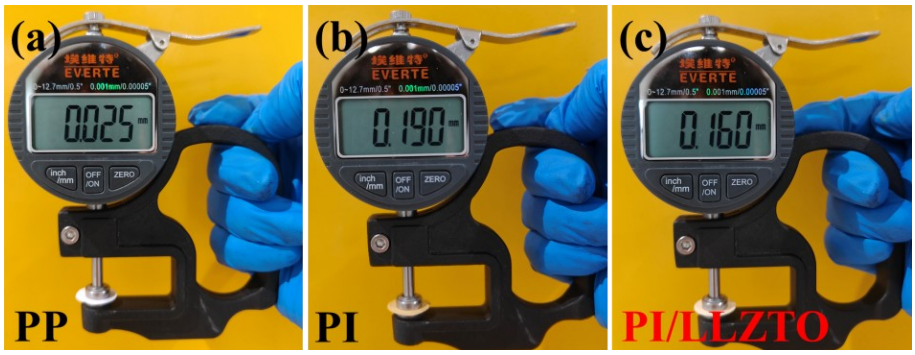


**Fig. S4.** Photograph of the thickness for the PP, PI, PI/LLZTO membranes.

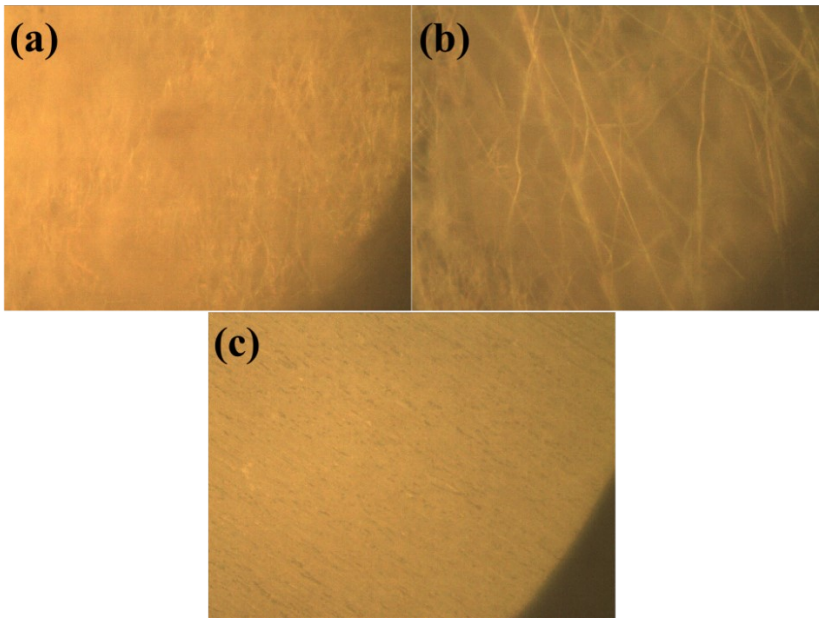


**Fig. S5.** The surface optical microscope images of (a) PI/LLZTO, (b) PI and (c) PP membrane.

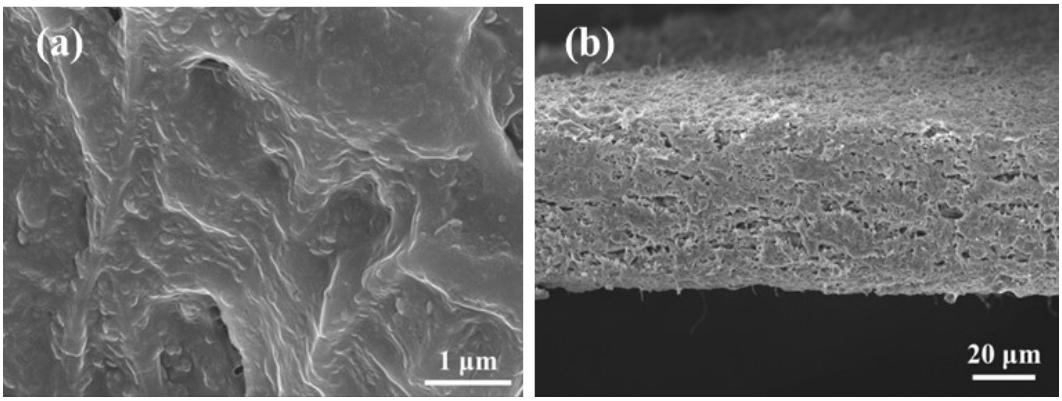


**Fig. S6.** SEM images (a) Surface morphology of PI/GPE membrane and (b) cross-sectional morphology of PI/LLZTO/GPE membrane.

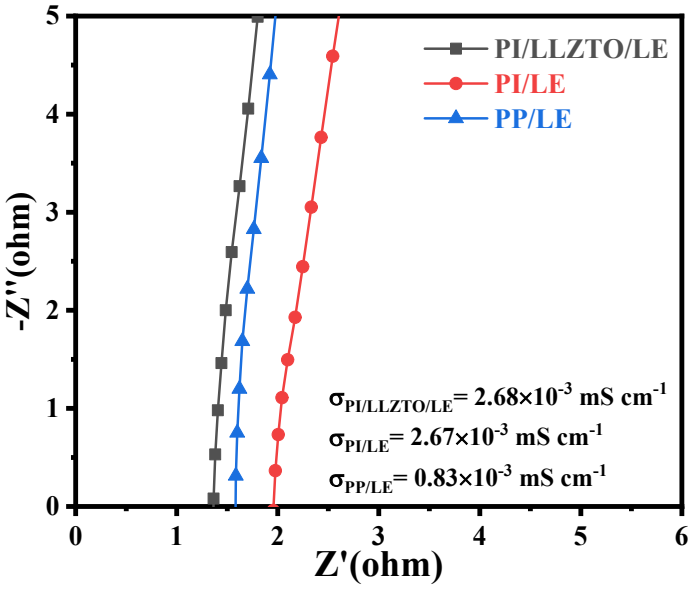


**Fig. S7.** Ionic conductivity of the PP, PI and PI/LLZTO in EC/DMC/EMC-$LiPF_6$ liquid electrolyte.

**Table S1** Porosity of the PP, PI and PI/LLZTO membrane.

| Sample | PP | PI | PI/LLZTO |
|---|---|---|---|
| Porosity (%) | 40.5 | 74.7 | 75.7 |

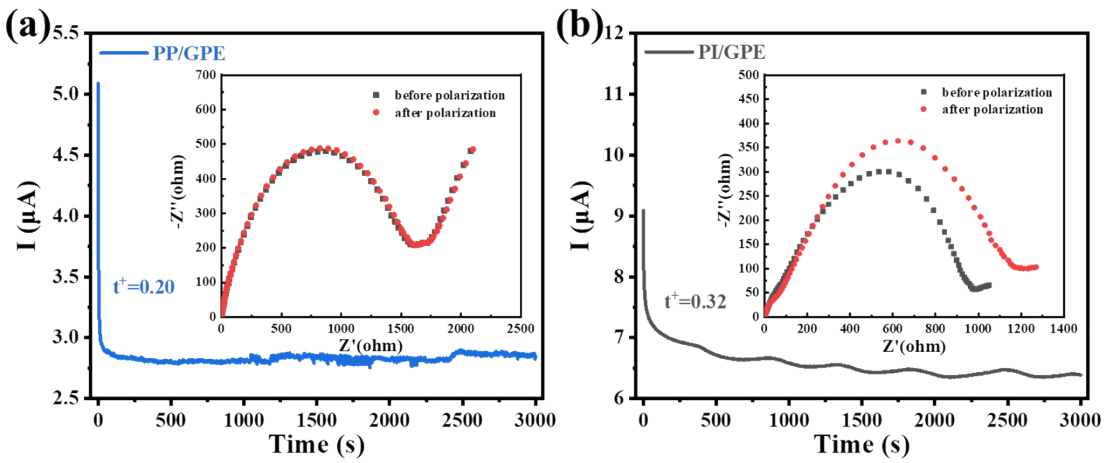


**Fig. S8.** Current-time curve of symmetrical (a) Li|PP/GPE|Li cell and (b) Li|PI/GPE|Li at a DC polarization of 10 mV, the inset shows the EIS of the cell before and after polarization.

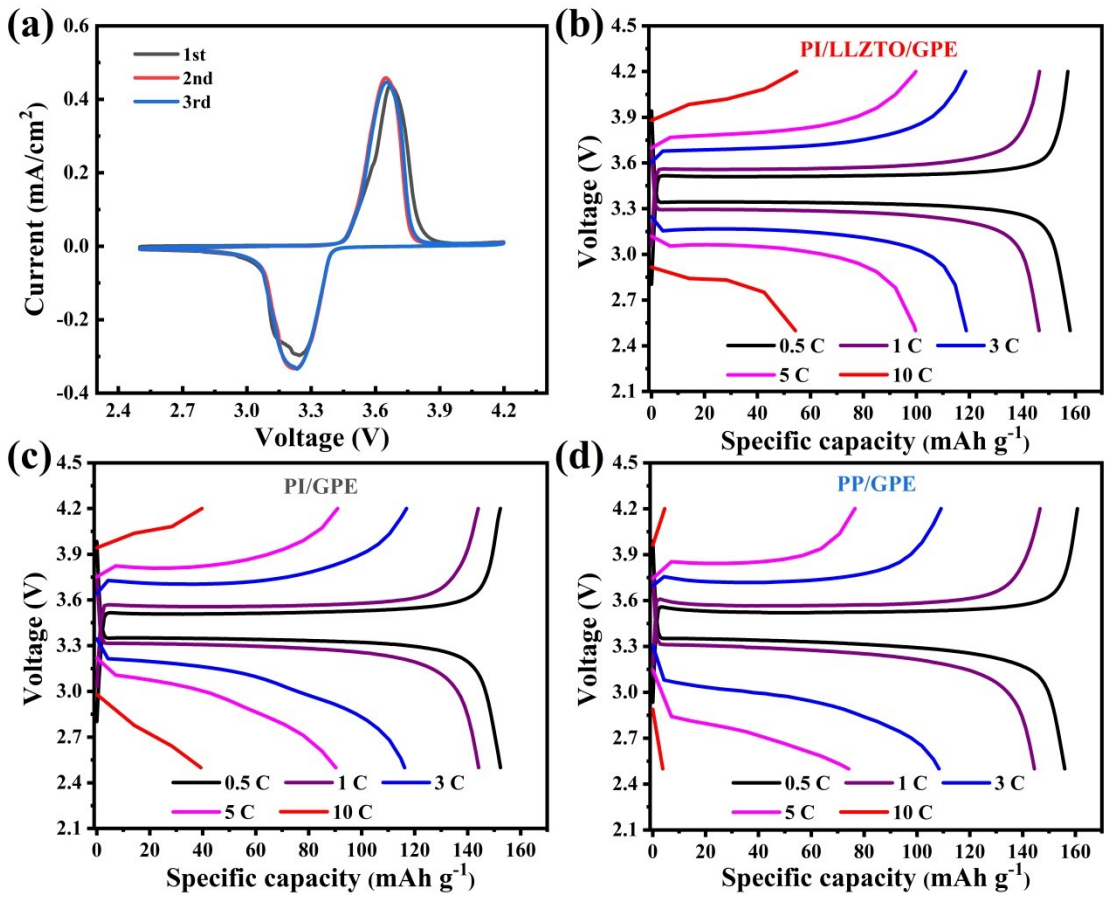


**Fig.S9.** (a) Cyclic voltammograms of Li|PI/LLZTO/GPE|LFP cell at a scan rate of 0.1 mV $s^{-1}$; charge/discharge voltage curves of (b) Li|PI/LLZTO/GPE|LFP cell, (c) Li|PI/GPE|LFP cell and (d) Li|PP/GPE|Li cell at different rates.

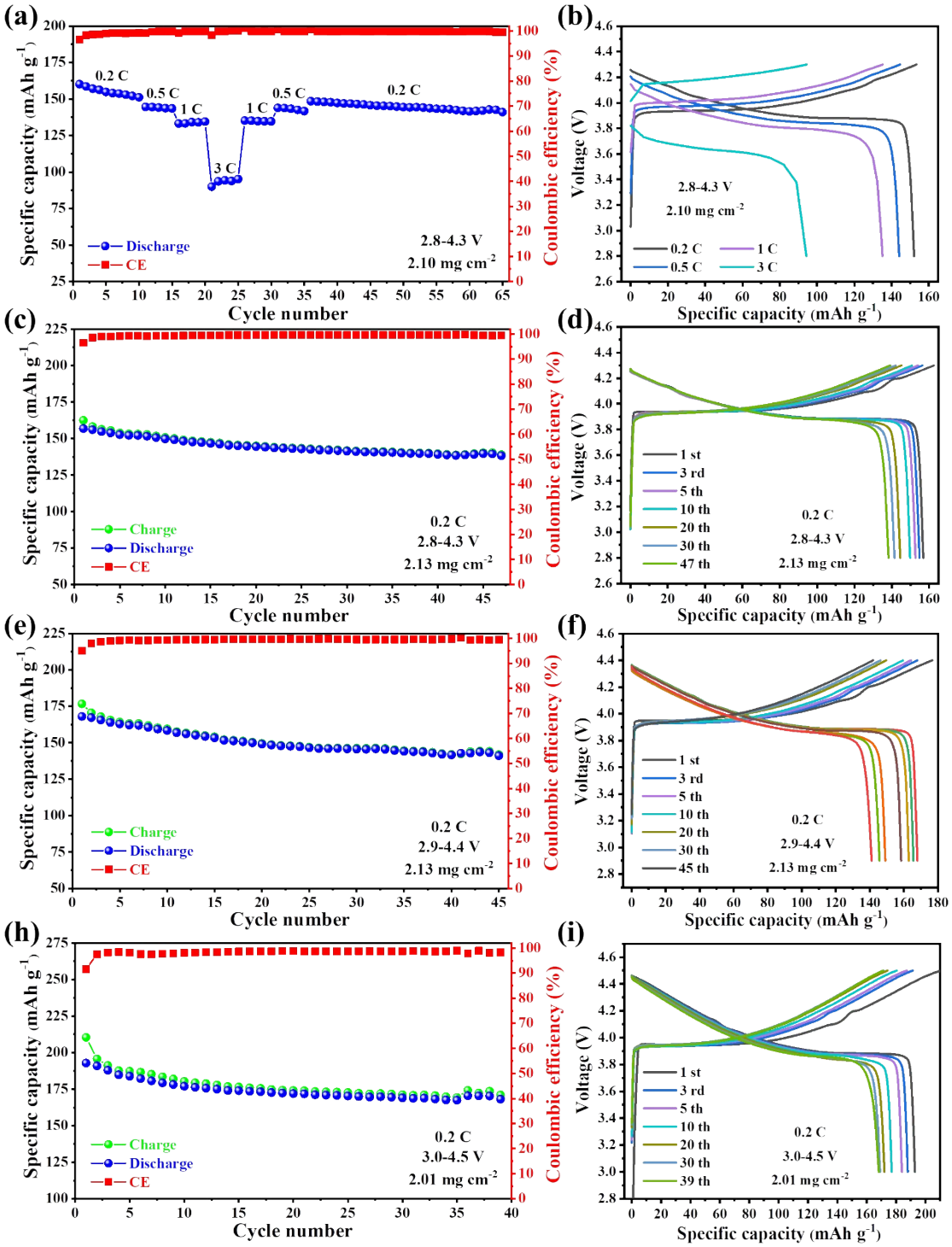


**Fig. S10.** The Li|PI/LLZTO|LCO cell of (a) rate performance form 0.2 C to 3 C and (b) charge-discharge curves. Cycling performance of Li|PI/LLZTO|LCO cells with a cut-off voltage of (c) 2.8-4.3 V, (e) 2.9-4.4 V and (h) 3.0-4.5 V; (d), (f) and (i) are their charge-discharge curves respectively. All cells were test at room temperature.

**Table S2.** Recent reported work with similar gel polymer electrolyte

| Reference | Ionic conductivity | $Li^+$ transfer number | Rate performance | Electrochemical window |
|---|---|---|---|---|
| Ref.3 | 7.60 mS $cm^{-1}$ | 0.43 | LFP/Li (2 C, 110 mAh $g^{-1}$) | 4.3 V vs $Li/Li^+$ |
| Ref.1 | 1.25 mS $cm^{-1}$ | 0.57 | LCO/Li (2 C, 100 mAh $g^{-1}$) | 5.1 V vs $Li/Li^+$ |
| Ref.4 | 6.90 mS $cm^{-1}$ | 0.51 | LCO/Li (2 C, 100 mAh $g^{-1}$) | 5.3 V vs $Li/Li^+$ |
| Ref.5 | 0.14 mS $cm^{-1}$ | 0.97 | LFP/Li (1 C, 130 mAh $g^{-1}$) | 5.2 V vs $Li/Li^+$ |
| Ref.6 | 0.45 mS $cm^{-1}$ | 0.72 | LCO/Li (5 C, 64 mAh $g^{-1}$) | 4.8 V vs $Li/Li^+$ |
| Ref.7 | 0.27 mS $cm^{-1}$ | 0.68 | LFP/Li (3 C, 89 mAh $g^{-1}$) | 4.2 V vs $Li/Li^+$ |
| Ref.8 | 0.82 mS $cm^{-1}$ | 0.55 | LFP/Li (2 C, 76 mAh $g^{-1}$) | 4.8 V vs $Li/Li^+$ |
| **This work** | **1.87 mS $cm^{-1}$** | **0.64** | **LFP/Li (5 C, 100 mAh $g^{-1}$ 10 C, 56 mAh $g^{-1}$)** | **4.5 V vs $Li/Li^+$** |

## References


1. D. Cai, X. Qi, J. Xiang, X. Wu, Z. Li, X. Luo, X. Wang, X. Xia, C. Gu and J. Tu, *Chemical Engineering Journal*, 2022, **435**.
2. Y. Huang, S. Liu, Q. Chen, K. Jiao, B. Ding and J. Yan, *Advanced Functional Materials*, 2022, **32**.
3. Q. Wang, X. Xu, B. Hong, M. Bai, J. Li, Z. Zhang and Y. Lai, *Chemical Engineering Journal*, 2022, **428**.
4. Q. Zhou, C. Fu, R. Li, X. Zhang, B. Xie, Y. Gao, G. Yin and P. Zuo, *Chemical Engineering Journal*, 2022, **437**.
5. Z. Li, Y. Liu, X. Liang, M. Yu, B. Liu, Z. Sun, W. Hu and G. Zhu, *Journal of Materials Chemistry A*, 2023, **11**, 1766-1773.
6. Y. Wang, L. Fu, L. Shi, Z. Wang, J. Zhu, Y. Zhao and S. Yuan, *ACS Appl Mater Interfaces*, 2019, **11**, 5168-5175.
7. D. Jia, Y. Cui, Q. Liu, M. Zhou, J. Huang, R. Liu, S. Liu, B. Zheng, Y. Zhu and D. Wu, *Materials Today Nano*, 2021, **15**.
8. Y. Chen, Y. Zhang, W. Liang, H. Xu, Z. Dong, J. Xu and C. Lei, *Chem Commun (Camb)*, 2022, **58**, 11961-11964.